The Nanoscale Electrical Damage Mechanism of $Ge_2Sb_2Te_5$ Phase-Change Films Discovered by Conductive Atomic Force Microscopy

Xionghu Xu, Ming Li, Shubing Li, Anyang Cui, Menghan Deng, Kai Jiang, Liangqing Zhu, Liyan Shang, Junhao Chu, and Zhigao Hu

***Abstract*—We study the nanoscale electrical damage of $Ge_2Sb_2Te_5$ (GST) phase-change films during crystallization by conductive atomic force microscopy (C-AFM) and Raman spectra. Amorphous GST (*a*-GST) can be converted to crystalline GST (*c*-GST) by applying an exciting direct current (DC) bias (8 V) between the tip and the GST surface. Furthermore, as film thickness increased, the electrical-induced region of GST films revealed a gradual increase in electrical damage and improved crystallinity. It shows that GST films with a thickness of 70 nm have a better crystallization ratio of 20.5 % and less electrical damage with a volume expansion rate of 19.1±6.5%.**

***Index Terms*—C-AFM, GST films, phase-change, Joule heat, crystallinity.**

I. Introduction

PHASE-CHANGE materials (PCMs), such as the chalcogenide $Ge_2Sb_2Te_5$ (GST), are of great interest because of fast and reversible transformations between the amorphous and crystalline phases [1], [2], [3], [4], [5]. As a result of the low power consumption, rapid read/write speed, and extended cycling endurance, PCMs offer considerable potential in nonvolatile electronic memory devices, such as phase-change random access memory (PCRAM). [6], [7], [8], [9], [10] As we know, most of PCMs can be transformed between amorphous and crystalline states using a reasonable temporal modulation of an electrical or optical pulse [11], [12], [13], [14], [15]. The optical, electrical, and mechanical properties of the two states differ significantly, which is useful in optoelectronic technology [16], [17], [18]. However, the contemporary phase-change memories confront significant problems, such as phase segregation, atomic migration [19], [20], [21], [22]. These issues can wreak havoc on the efficient usage of technology. As a result, a better understanding of the phase-change mechanism is critical for the development of microelectronic and optoelectronic applications.

Since shrinking the feature size of electronic devices is a good approach to improve performance in terms of increased storage density and reduced power consumption, it is vital to study the mechanism of phase shift at the nanoscale dimension. Fortunately, as a sophisticated equipment with atomic resolution, atomic force microscopy (AFM) is well suited for this study aim. Furthermore, conductive atomic force microscopy (C-AFM), which can be used in recording on phase-change films, [23], [24], [25] is a powerful tool for detecting electrical changes at the nanoscale level. References [26], [27], and Cecchini et al. [28] studied the nanoscratching process on the crystalline GST (*c*-GST) with a fixed constant force of 100-300 μN along the z direction. Anbarasu et al. [29] also studied the threshold switching characteristics of $GeTe_6$ films using C-AFM. Wright et al. demonstrated the design nanometer-scale electronic phase-change devices by simulation based on the ability of C-AFM to induce the GST films at the nanoscale. [30], [31] however, the electrical damage on *a*-GST caused by C-AFM is unclear during the crystallization.

Herein, C-AFM was utilized to analyze the electrical properties and electrical damage of GST films under a local electric field at the nanoscale dimension. Due to the advantages of ultra-high resolution and current sensitivity of C-AFM, the variation of topograph and electrical properties of GST films can be obtained simultaneously. The crystallization of GST

Manuscript received 10 November 2022; revised 4 January 2023; accepted 12 January 2023. Date of publication 16 January 2023; date of current version 24 February 2023. This work was supported in part by the National Natural Science Foundation of China under Grant 62090013, Grant 61974043, and Grant 61974044; in part by the National Key Research and Development Program of China under Grant 2019YFB2203403; in part by the Projects of Science and Technology Commission of Shanghai Municipality under Grant 21JC1402100 and Grant 19511120100; and in part by the Program for Professor of Special Appointment (Eastern Scholar) at Shanghai Institutions of Higher Learning. The review of this letter was arranged by Editor U. Ganguly. *(Corresponding authors: Liangqing Zhu; Zhigao Hu.)*

Xionghu Xu, Ming Li, Shubing Li, Anyang Cui, Menghan Deng, Kai Jiang, Liangqing Zhu, and Liyan Shang are with the Technical Center for Multifunctional Magneto-Optical Spectroscopy (Shanghai), Engineering Research Center of Nanophotonics and Advanced Instrument (Ministry of Education), Department of Physics, School of Physics and Electronic Science, East China Normal University, Shanghai 200241, China (e-mail: lqzhu@ee.ecnu.edu.cn).

Junhao Chu and Zhigao Hu are with the Technical Center for Multifunctional Magneto-Optical Spectroscopy (Shanghai), Engineering Research Center of Nanophotonics and Advanced Instrument (Ministry of Education), Department of Physics, School of Physics and Electronic Science, East China Normal University, Shanghai 200241, China, and also with the Collaborative Innovation Center of Extreme Optics, Shanxi University, Taiyuan, Shanxi 030006, China (e-mail: zghu@ee.ecnu.edu.cn).

Color versions of one or more figures in this letter are available at https://doi.org/10.1109/LED.2023.3237230.

Digital Object Identifier 10.1109/LED.2023.3237230

0741-3106 © 2023 IEEE. Personal use is permitted, but republication/redistribution requires IEEE permission.
See https://www.ieee.org/publications/rights/index.html for more information.

Authorized licensed use limited to: East China Normal University. Downloaded on February 27,2023 at 01:32:12 UTC from IEEE Xplore. Restrictions apply.

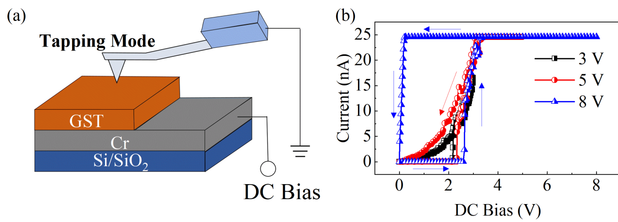

Fig. 1. (a) Schematic diagram of the sample structure. (b) Current-voltage curve of GST/Cr/SiO_2/Si arrangement structure with PtSi-coated C-AFM tip as top electrode.

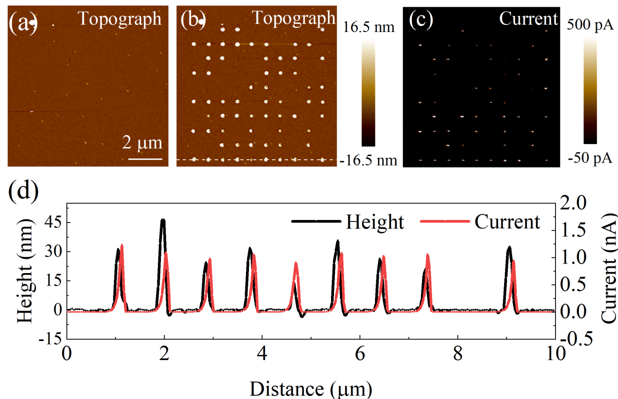

Fig. 2. (a) An original AFM topograph image of an *a*-GST film. (b) A topograph image and (c) a current image of a C-AFM tip-induced 10 × 10 array of conductive points in an *a*-GST film after set voltage with 8 V at a readout voltage of 1 V. (d) A height profile plotted and a current profile plotted along with the white dashed line in (b).

films can be observed by applying a strong electric field to the surface of GST films with C-AFM. There was a local-area surface protrusion (electrical damage caused by Joule heat) and greater electrical conductivity on the tip-induced area of GST films after GST films transitioned from amorphous to crystalline state induced by C-AFM tip. Subsequently, Kelvin probe force microscope (KPFM) tests and *in-situ* Raman measurements were done to validate the transition from amorphous state to crystalline state of GST films.

II. Experimental

The Cr bottom electrodes (100 nm) were deposited on SiO_2-covered Si (100) substrates by thermal evaporation, then the *a*-GST films (70 nm) were grown at room temperature by pulsed laser deposition (PLD) on it [32]. To minimize the impact caused by contact mode or excessive tip force. A commercial AFM system (Bruker AFMs: Dimension Icon with PeakForce TUNA mode) with a "SCM-PTSI" AFM tip was employed to analyze the electrical characteristics and topography of GST films. The diameter of the AFM tip is 20 nm, the spring constant of the cantilever is 2.8 N m^{-1} (with the force of 50-100 nN). The current sensitivity of C-AFM is 2 nA/V.

Additionally, *in-situ* Raman measurements were performed with a green laser at 532 nm. A higher laser intensity could be another trigger that causes the GST films to crystallize, hence 0.1 mW/mm^2 of laser intensity was chosen. The schematic diagram of the experimental configuration is shown in Fig. 1(a). The variable bias voltage was applied between the bottom Cr layer electrode and the top electrode consisting of an AFM tip. At the nanoscale region, the voltage was directly applied to the GST films by the conductive tip to achieve electrical stimulation, the power consumed at the nanoscale area grows as the voltage applied increases. To explore the transformation from *a*-GST to *c*-GST, different voltage clockwise-cycling (3 V, 5 V, 8 V) was placed to this circuit loop in 1 second, with the current limited in the range of 0 to 25 nA.

III. Results and Discussion

A representative measured I-V characteristic of the SCM-PTSI/GST/Cr stack is shown in Fig. 1(b). Different from the standard electrical test, it cannot get the specific resistance values of the high resistance state and the low resistance state using C-AFM. However, we can still see that the GST film achieves a stable and low resistance crystalline state after 8V set in Fig. 1(b). The GST film initially exhibits a high resistance state (OFF state), suggesting that the conductive bridge had not yet formed. When the set voltage set as 3 V or 5 V, there will be a transition from the *a*-GST OFF state to *a*-GST ON state rather than phase change. Sb or Te ions will migrate in the amorphous state, leading to the formation of the conductive bridge. In the absence of an electric field, the conductive bridge will also collapse.

The reverse curve (from 8 V to 0 V) showed a lowered resistance condition when the set voltage was 8 V. Sufficient power was supplied to realize the transition from *a*-GST to *c*-GST, resulting in a large change of resistivity, as shown in Fig. 1(b). This is because that the defects are reduced when large grains emerge, which causes the rate of carrier recombination to decrease. Resistance will ultimately decrease as the number of carriers rises [33], [34], [35], [36]. However, enough Joule heat may induce irreversible electrical damage on the GST films, resulting in a "height growth".

In order to visualize the nanoscale crystallization and electrical damage of GST, the topograph and current image were simultaneously captured by C-AFM at a readout voltage of 1 V. In theory, the volume of GST film will become smaller after the transition from amorphous state to crystalline state, however, due to the influence of electric field and Joule heat, the results of *c*-GST showed an opposing volume change as shown in Fig. 2(b) and (d). These protrusions (bright spots) formed because the energy generated by Joule heat was high enough to melt the nearby amorphous GST into liquid form [37], [38]. The protrusions could be formed during the nucleation and growth of *c*-GST since the upper surface was unbound according to the Ovshinsky's nucleation hypothesis [1], [37], [39]. Interestingly, the size of the current points in Fig. 2(c) is smaller than that of the topograph points, demonstrating the fact that the presence of pores will break down the conductive channel in the vertical direction and generate an invalid crystallization area.

To demonstrate the crystallization of GST film following electrical stimulation triggered by the C-AFM tip. A 20 × 20 array points were set with 8 V voltages on the *a*-GST film, as shown in Fig. 3(a). The conductivity has been changed after induced by C-AFM. The surface potential must be different between *a*-GST and *c*-GST. As shown in Fig. 3(b), the *in-situ* potential image shows that the surface potential of the tip-induced area is 0.15 V, which is higher than the potential of the *a*-GST sounding using KPFM. This is because the *c*-GST has higher electrical conductance than that from *a*-GST.

Authorized licensed use limited to: East China Normal University. Downloaded on February 27,2023 at 01:32:12 UTC from IEEE Xplore. Restrictions apply.

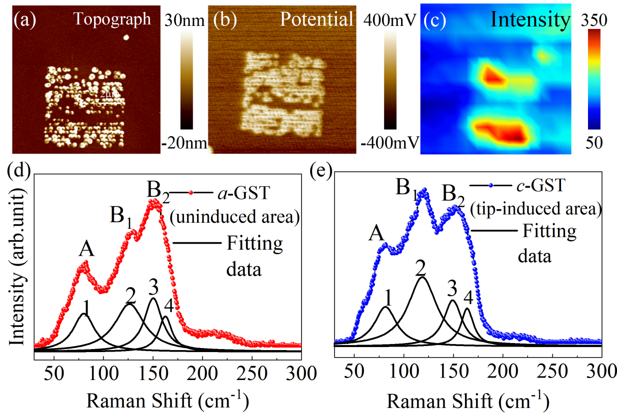

Fig. 3. (a) A topography image of a 20 × 20 array crystalline pattern on 70 nm *a*-GST film after 8 V set voltage. (b) Simultaneously recorded potential image of the tip-induced *a*-GST film using KPFM. (c) *In-situ* Raman mapping image for intensity from peak 2 of the fitting data. Raman spectra of (d) *a*-GST (uninduced area) and (e) *c*-GST (tip-induced area), including the fitting data to the Lorentz-Gaussian functions for each state.

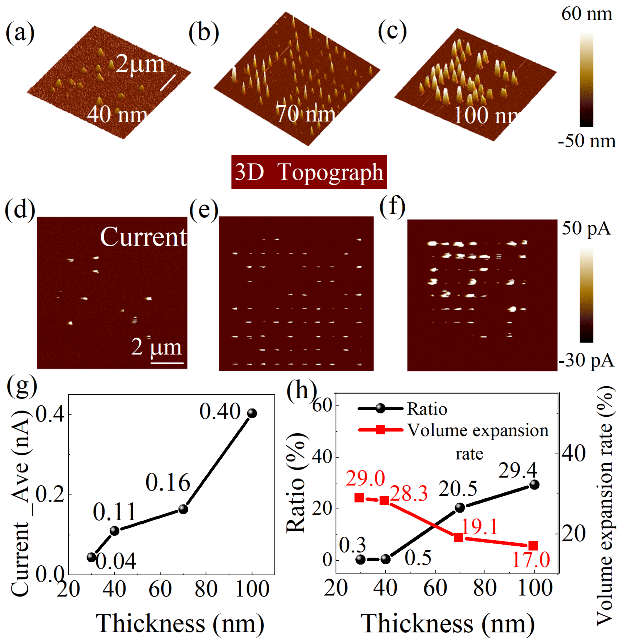

Fig. 4. Three-dimensional topograph images of electrical induced GST films with different thicknesses of (a) 40 nm, (b) 70 nm, (c) 100 nm. Their corresponding current images are given in (d), (e), and (f), respectively. (g) The average current over the tip-induced area on GST films, (h) the ratio of effective crystallization and the volume expansion ratio as a function of the thickness of GST films, respectively.

On the other hand, Raman scattering spectra is an effective measurement to analyze the structural variation of the GST films [40], [41]. The Raman spectra of the uninduced area and tip-induced area of the GST film are shown in Fig. 3(d) and (e), respectively. The Raman spectra can be regarded as two broadening peaks marked with peak A and B, respectively. The lower frequency peak, namely peak A, contains the F2 mode and the E mode of the $GeTe_4$ tetrahedra vibrations. However, there is a shift to a higher frequency (from 150.4 cm^{-1} to 158.1 cm^{-1}) of peak B_2, which is attributed to the substitution of Sb-Te band vibrations for Te-Te band vibrations after electrically-induced crystallization. Notably, there is a significantly increase of the intensity of peak 2, as shown in Fig. 3 (c), which can be attributed to the increasing GeTe content in the $GeTe_{4-n}Ge_n$ ($n = 1$, 2) tetrahedra with the tetrahedra transforming into defective octahedra.

To further study the electrical damage and crystallinity of GST film caused by C-AFM conductive tip. The GST films with different thicknesses were taken to check the same electrical inducement. As illustrated in Fig. 4, the GST films with higher thicknesses exhibited bigger protrusion sizes and improved crystallinity. However, when the thickness of GST film is beyond 160 nm, there is no change on *a*-GST films (not shown). This is due to the electric field's inability to stimulate the creation of conductive filaments beyond this thickness. Because the protrusions are shaped like cones, the volume expansion rate (r) can be written as:

$$r = \frac{V_{spot}}{V_{induce}}, V_{spot} = \frac{\pi}{3}(\frac{D}{2})^2\ H, V_{induce} = \pi(\frac{D}{2})^2 t$$

where V_{spot} and V_{induce} are volume of spot and induced cylinder area, respectively. H and D are height and diameter of spot, and t is the thickness of GST film, respectively.

It's interesting to note that the rate of electrical damage lowers as thickness increases. Additionally, as shown in Fig. 4(g), the average current of the GST film increases with thickness. The ratio of the effective crystallization area to the protrusion area can describe the ratio of effective crystallization, as shown in Fig. 4(h). It can be concluded that The GST films with a thickness of 70 nm have a smaller volume expansion (19.1 ± 6.5 %) and better crystallization (20.5%). The balance between two parameters can be helpful for the GST phase-change based optoelectronic and microelectronic device designing.

IV. Conclusion

In conclusion, we used C-AFM to study the nanoscale crystallization of *a*-GST films of varying thicknesses deposited by PLD. KPFM and *in-situ* Raman measurements were performed to prove the formation of *c*-GST. By using C-AFM, we have realized the crystallization of GST films at the nanoscale area. The crystallinity and electrical damage of GST films with different thicknesses are performed. Though the thicker GST films have a better crystallization ratio, the rate of electrical damage increases; hence, the thickness of the phase change layer must be chosen carefully. The results show that the GST film with the thickness of 70 nm is with a better crystallization ratio (20.5 %) and a lower electrical damage rate with a volume expansion rate (19.1 ± 6.5 %). The current research contributes to a better knowledge of the performance mechanism of GST PCM devices.

References

[1] S. R. Ovshinsky, "Reversible electrical switching phenomena in disordered structures," *Phys. Rev. Lett.*, vol. 21, no. 20, pp. 1450–1453, 1968, doi: 10.1103/PhysRevLett.21.1450.

[2] I. Friedrich, V. Weidenhof, S. Lenk, and M. Wuttig, "Morphology and structure of laser-modified $Ge_2Sb_2Te_5$ films studied by transmission electron microscopy," *Thin Solid Films*, vol. 389, nos. 1–2, pp. 239–244, Feb. 2001, doi: 10.1016/S0040-6090(01)00891-4.

[3] R. Huang, K. Sun, K. S. Kiang, R. Chen, Y. Wang, B. Gholipour, D. W. Hewak, and C. H. De Groot, "Contact resistance measurement of $Ge_2Sb_2Te_5$ phase change material to TiN electrode by spacer etched nanowire," *Semicond. Sci. Technol.*, vol. 29, no. 9, Jul. 2014, Art. no. 095003, doi: 10.1088/0268-1242/29/9/095003.

Authorized licensed use limited to: East China Normal University. Downloaded on February 27,2023 at 01:32:12 UTC from IEEE Xplore. Restrictions apply.

[4] H. C. Lee, J. H. Jeong, and D. J. Choi, “Characterization of phase-change behavior of a $Ge_2Sb_2Te_5$ thin film using finely controlled electrical pulses for switching,” *Semicond. Sci. Technol.*, vol. 31, no. 9, Aug. 2016, Art. no. 095006, doi: 10.1088/0268-1242/31/9/095006.

[5] P. Singh, P. Sharma, V. Sharma, and A. Thakur, “Linear and non-linear optical properties of Ag-doped $Ge_2Sb_2Te_5$ thin films estimated by single transmission spectra,” *Semicond. Sci. Technol.*, vol. 32, no. 4, Mar. 2017, Art. no. 045015, doi: 10.1088/1361-6641/aa5ee0.

[6] M. H. R. Lankhorst, B. W. S. M. M. Ketelaars, and R. A. M. Wolters, “Low-cost and nanoscale non-volatile memory concept for future silicon chips,” *Nature Mater.*, vol. 4, pp. 347–352, Mar. 2005, doi: 10.1038/nmat1350.

[7] H. S. P. Wong, S. Raoux, S. Kim, J. L. Liang, J. P. Reifenberg, B. Rajendran, M. Asheghi, and K. E. Goodson, “Phase change memory,” *Proc. IEEE*, vol. 98, no. 12, pp. 2201–2227, Dec. 2010, doi: 10.1109/JPROC.2010.2070050.

[8] T. Tuma, A. Pantazi, M. Le Gallo, A. Sebastian, and E. Eleftheriou, “Stochastic phase-change neurons,” *Nat. Nanotechnol.*, vol. 11, no. 8, pp. 693–699, Aug. 2016, doi: 10.1038/Nnano.2016.70.

[9] N. K. Upadhyay, H. Jiang, Z. Wang, S. Asapu, Q. Xia, and J. J. Yang, “Emerging memory devices for neuromorphic computing,” *Adv. Mater. Technol.*, vol. 4, no. 4, Apr. 2019, Art. no. 1800589, doi: 10.1002/admt.201800589.

[10] N. Youngblood, C. Rios, E. Gemo, J. Feldmann, Z. G. Cheng, A. Baldycheva, W. H. P. Pernice, C. D. Wright, and H. Bhaskaran, “Tunable volatility of $Ge_2Sb_2Te_5$ in integrated photonics,” *Adv. Funct. Mater.*, vol. 29, no. 11, Mar. 2019, Art. no. 1807571, doi: 10.1002/adfm.201807571.

[11] M. Wuttig and N. Yamada, “Phase-change materials for rewriteable data storage,” *Nature Mater.*, vol. 6, pp. 824–832, Nov. 2007, doi: 10.1038/nmat2009.

[12] S. Guo, Z. G. Hu, X. L. Ji, T. Huang, X. L. Zhang, L. C. Wu, Z. T. Song, and J. H. Chu, “Temperature and concentration dependent crystallization behavior of $Ge_2Sb_2Te_5$ phase change films: Tungsten doping effects,” *RSC Adv.*, vol. 4, no. 100, pp. 57218–57222, Oct. 2014, doi: 10.1039/c4ra08790a.

[13] G. Rodriguez-Hernandez, P. Hosseini, C. Rios, C. D. Wright, and H. Bhaskaran, “Mixed-mode electro-optical operation of $Ge_2Sb_2Te_5$ nanoscale crossbar devices,” *Adv. Electron. Mater.*, vol. 3, no. 8, Aug. 2017, Art. no. 1700079, doi: 10.1002/aelm.201700079.

[14] M. Choi, H. Choi, J. Ahn, and Y. T. Kim, “Material design for $Ge_2Sb_2Te_5$ phase-change material with thermal stability and lattice distortion,” *Scr. Mater.*, vol. 170, pp. 16–19, Sep. 2019, doi: 10.1016/j.scriptamat.2019.05.024.

[15] T. Fan, F. R. Liu, W. Q. Li, J. C. Guo, Y. H. Wang, N. X. Sun, and F. Liu, “The crystallization behavior of amorphous $Ge_2Sb_2Te_5$ films induced by a multi-pulsed nanosecond laser,” *Semicond. Sci. Technol.*, vol. 32, no. 9, Sep. 2017, Art. no. 095003, doi: 10.1088/1361-6641/aa7c4e.

[16] N. Yamada, “Origin, secret, and application of the ideal phase-change material GeSbTe,” *Phys. Status Solidi b*, vol. 249, no. 10, pp. 1837–1842, Oct. 2012, doi: 10.1002/pssb.201200618.

[17] N. El-Hinnawy, P. Borodulin, B. Wagner, M. R. King, J. S. Mason, E. B. Jones, S. McLaughlin, V. Veliadis, M. Snook, M. E. Sherwin, R. S. Howell, R. M. Young, and M. J. Lee, “A four-terminal, inline, chalcogenide phase-change RF switch using an independent resistive heater for thermal actuation,” *IEEE Electron Device Lett.*, vol. 34, no. 10, pp. 1313–1315, Oct. 2013, doi: 10.1109/LED.2013.2278816.

[18] T. Singh and R. R. Mansour, “Non-volatile multiport DC–30 GHz monolithically integrated phase-change transfer switches,” *IEEE Electron Device Lett.*, vol. 42, no. 6, pp. 867–870, Jun. 2021, doi: 10.1109/LED.2021.3076047.

[19] T. Y. Yang, I. M. Park, B. J. Kim, and Y. C. Joo, “Atomic migration in molten and crystalline $Ge_2Sb_2Te_5$ under high electric field,” *Appl. Phys. Lett.*, vol. 95, no. 3, Jul. 2009, Art. no. 032104, doi: 10.1063/1.3184584.

[20] D. Kang, D. Lee, H. M. Kim, S. W. Nam, M. H. Kwon, and K. B. Kim, “Analysis of the electric field induced elemental separation of $Ge_2Sb_2Te_5$ by transmission electron microscopy,” *Appl. Phys. Lett.*, vol. 95, no. 1, Jul. 2009, Art. no. 011904, doi: 10.1063/1.3168517.

[21] J. T. Li, Y. Y. Xia, B. Liu, G. M. Feng, Z. T. Song, D. Gao, Z. Xu, W. W. Wang, Y. P. Chan, and S. L. Feng, “Direct evidence of reactive ion etching induced damages in $Ge_2Sb_2Te_5$ based on different halogen plasmas,” *Appl. Surf. Sci.*, vol. 378, pp. 163–166, Mar. 2016, doi: 10.1016/j.apsusc.2016.03.122.

[22] M. Agati, C. Gay, D. Benoit, and A. Claverie, “Effects of surface oxidation on the crystallization characteristics of Ge-rich Ge-Sb-Te alloys thin films,” *Appl. Surf. Sci.*, vol. 518, Jul. 2020, Art. no. 146227, doi: 10.1016/j.apsusc.2020.146227.

[23] H. Kado and T. Tohda, “Nanometer-scale recording on chalcogenide films with an atomic force microscope,” *Appl. Phys. Lett.*, vol. 66, no. 22, pp. 2961–2962, May 1995, doi: 10.1063/1.114243.

[24] H. Kado and T. Tohda, “Nanometer-scale erasable recording using atomic force microscope on phase change media,” *Jpn. J. Appl. Phys.*, vol. 36, pp. 523–525, Jan. 1997, doi: 10.1143/JJAP.36.523.

[25] H. F. Hamann, M. O’Boyle, Y. C. Martin, M. Rooks, and H. K. Wickramasinghe, “Ultra-high-density phase-change storage and memory,” *Nature Mater.*, vol. 5, pp. 383–387, Apr. 2006, doi: 10.1038/nmat1627.

[26] R. Pandian, B. J. Kooi, G. Palasantzas, J. T. M. De Hosson, and A. Pauza, “Nanoscale electrolytic switching in phase-change chalcogenide films,” *Adv. Mater.*, vol. 19, pp. 4431–4437, Dec. 2007, doi: 10.1002/adma.200700904.

[27] Y. Jung, S. W. Nam, and R. Agarwal, “High-resolution transmission electron microscopy study of electrically-driven reversible phase change in $Ge_2Sb_2Te_5$ nanowires,” *Nano. Lett.*, vol. 11, no. 3, pp. 1364–1368, Jan. 2011, doi: 10.1021/nl104537c.

[28] R. Cecchini, J. J. Benítez, J. C. Sánchez-López, and A. Fernández, “Nanoscale mechanically induced structural and electrical changes in $Ge_2Sb_2Te_5$ films,” *J. Appl. Phys.*, vol. 111, no. 1, Jan. 2012, Art. no. 016101, doi: 10.1063/1.3673592.

[29] A. Manivannan, S. K. Myana, K. Miriyala, S. Sahu, and R. Ramadurai, “Low power ovonic threshold switching characteristics of thin $GeTe_6$ films using conductive atomic force microscopy,” *Appl. Phys. Lett.*, vol. 105, no. 24, Dec. 2014, Art. no. 243501, doi: 10.1063/1.4904412.

[30] C. D. Wright, L. Wang, P. Shah, M. M. Aziz, E. Varesi, R. Bez, M. Moroni, and F. Cazzaniga, “The design of rewritable ultrahigh density scanning-probe phase-change memories,” *IEEE Trans. Nanotechnol.*, vol. 10, no. 4, pp. 900–912, Jul. 2011, doi: 10.1109/TNANO.2010.2089638.

[31] C. D. Wright, P. Hosseini, and J. A. V. Diosdado, “Beyond von-Neumann computing with nanoscale phase-change memory devices,” *Adv. Funct. Mater.*, vol. 23, no. 18, pp. 2248–2254, Dec. 2012, doi: 10.1002/adfm.201202383.

[32] M. Li, M. Z. Xie, H. Ji, J. Y. Zhou, K. Jiang, L. Y. Shang, Y. W. Li, Z. G. Hu, and J. H. Chu, “PLD-derived $Ge_2Sb_2Te_5$ phase-change films with extreme bending stability for flexible device applications,” *Appl. Phys. Lett.*, vol. 116, no. 16, Apr. 2020, Art. no. 162102, doi: 10.1063/5.0001348.

[33] X. Wang, T. Liu, Y. Lu, Q. Li, R. Guo, X. Jiao, and X. Xu, “Nucleation switching in phase change memory,” *Appl. Phys. Lett.*, vol. 90, no. 12, Mar. 2007, Art. no. 123504, doi: 10.1063/1.2715024.

[34] S. R. Ovshinsky, “Localized states in the gap of amorphous semiconductors,” *Phys. Rev. Lett.*, vol. 36, no. 24, pp. 1469–1472, Jun. 1976, doi: 10.1103/PhysRevLett.36.1469.

[35] D. Adler, H. K. Henisch, and S. N. Mott, “The mechanism of threshold switching in amorphous alloys,” *Rev. Mod. Phys.*, vol. 50, pp. 209–220, Apr. 1978, doi: 10.1103/RevModPhys.50.209.

[36] A. Pirovano, A. L. Lacaita, A. Benvenuti, F. Pellizzer, and R. Bez, “Electronic switching in phase-change memories,” *IEEE Trans. Electron Devices*, vol. 51, no. 3, pp. 452–459, Mar. 2004, doi: 10.1109/TED.2003.823243.

[37] J. Kalb, F. Spaepen, and M. Wuttig, “Atomic force microscopy measurements of crystal nucleation and growth rates in thin films of amorphous Te alloys,” *Appl. Phys. Lett.*, vol. 84, no. 25, pp. 5240–5242, Apr. 2004, doi: 10.1063/1.1764591.

[38] J. Kim, “Nanoscale crystallization of phase change $Ge_2Sb_2Te_5$ film with AFM lithography,” *Scanning*, vol. 32, no. 5, pp. 320–326, Sep. 2010, doi: 10.1002/sca.20201.

[39] M. L. Tseng, B. H. Chen, C. H. Chu, C. M. Chang, W. C. Lin, N.-N. Chu, M. Mansuripur, A. Q. Liu, and D. P. Tsai, “Fabrication of phase-change chalcogenide $Ge_2Sb_2Te_5$ patterns by laser-induced forward transfer,” *Opt. Exp.*, vol. 19, no. 18, pp. 16975–16984, Aug. 2011, doi: 10.1364/OE.19.016975.

[40] S. Kozyukhin, M. Veres, H. P. Nguyen, A. Ingram, and V. Kudoyarova, “Structural changes in doped $Ge_2Sb_2Te_5$ thin films studied by Raman spectroscopy,” *Phys. Proc.*, vol. 44, pp. 82–90, Apr. 2013, doi: 10.1016/j.phpro.2013.04.011.

[41] P. Němec, A. Moreac, V. Nazabal, M. Pavlišta, J. Přikryl, and M. Frumar, “Ge-Sb-Te thin films deposited by pulsed laser: An ellipsometry and Raman scattering spectroscopy study,” *J. Appl. Phys.*, vol. 106, no. 10, Oct. 2009, Art. no. 103509, doi: 10.1063/1.3259435.

Authorized licensed use limited to: East China Normal University. Downloaded on February 27,2023 at 01:32:12 UTC from IEEE Xplore. Restrictions apply.